Thermal conductivity of an ultracold paramagnetic Bose gas

Reuben R. W. Wang ⬤ and John L. Bohn
JILA, University of Colorado, Boulder, Colorado 80309, USA

We analytically derive the transport tensor of thermal conductivity in an ultracold, but not yet quantum degenerate, gas of Bosonic lanthanide atoms using the Chapman-Enskog procedure. The tensor coefficients inherit an anisotropy from the anisotropic collision cross section for these dipolar species, manifest in their dependence on the dipole moment, dipole orientation, and *s*-wave scattering length. These functional dependences open up a pathway for control of macroscopic gas phenomena via tuning of the microscopic atomic interactions. As an illustrative example, we analyze the time evolution of a temperature hot spot which shows preferential heat diffusion orthogonal to the dipole orientation, a direct consequence of anisotropic thermal conduction.

I. INTRODUCTION

Ultracold gases of spin-polarized magnetic atoms, such as dysprosium and erbium, have led to a wealth of novel phenomena in the quantum degenerate regime, as reviewed recently in Ref. [1]. Far less studied is the regime of such gases just above the temperature of quantum degeneracy. In this regime, a small magnetic field can ensure that the atoms remain polarized, whereby the classical fluid equations of motion inherit anisotropy due to this polarization. In particular, the transport coefficients—the thermal conductivity and the viscosity—inherit an anisotropy from the microscopic collision dynamics of the scattering dipoles.

In certain cases, the results of this collisional anisotropy are well known. They have already been shown to result in anisotropic thermalization in normal-phase ultracold gases and can be used as a tool for measuring scattering lengths [2–10]. These experiments have been modeled using perturbation theory around the equilibrium Boltzmann distribution of a gas, an analysis that has proven highly successful. Following on such success, it seems worthwhile to present the systematic derivation of the continuum fluid equations of motion for an ultracold paramagnetic gas. The present paper takes the first step in this program by deriving the anisotropic thermal-conductivity tensor from the differential cross section in dipolar lanthanide gases [11]. This is done by means of the Chapman-Enskog formalism [12], leading to density-independent coefficients valid in the dilute regime [13].

We focus here on Bosonic samples, which also offer a quantum-mechanical *s*-wave scattering length a_s [14], tunable via a multitude of Fano-Feshbach resonances. Thus, the anisotropy of the heat-conduction tensor is under direct experimental control. We note that our results here are unlike studies in which anisotropic transport tensors arise due to internal degrees of freedom or long-range interactions [15], such as in systems of dilute plasmas [16–19] and ferrofluids [20,21].

The remainder of this paper is organized as follows: In Secs. II and III, we analytically derive the anisotropic transport tensor of thermal conductivity emergent from dipolar collisions. The continuum conservation equations are introduced in Sec. IV, permitting a model for fluid dynamics studies in ultracold gases. This model is used to study a simple experimental scenario of thermal diffusion of a temperature hot spot in Sec. V. Finally, a discussion and concluding remarks are given in Sec. VI.

II. THE CHAPMAN-ENSKOG PROCEDURE

The study of transport phenomena is mature and extensive, having applications in all fields of science and engineering [22–25]. Central to the analysis of transport are the equations of conservation and constitution, which describe the dynamics of state variables (e.g., mass, flow velocity, and energy) and their response to external stimuli. If only weakly perturbed, the response of a system is completely described by linear constitutive relations and the associated, medium-specific transport coefficients.

In the present context, we consider an ultracold, dilute gas of Bosonic lanthanide atoms in their spin-stretched ground state and in sufficient magnetic field that they remain in this ground state in spite of collisions. The gas is then paramagnetic, with the preferred spatial axis determined by the field direction. Moreover, we explicitly consider only temperatures above the critical temperature of Bose-Einstein condensation, so that the thermodynamics of the gas is governed by Maxwell-Boltzmann statistics. While we focus on magnetic atoms here, the results should, of course, be applicable to ultracold gases of polar molecules.

In such a gas, local equilibrium occurs by means of dipolar collisions parameterized by the scattering length a and magnetic dipole length $a_d = C_{dd} m / (8\pi \hbar^2)$, where $C_{dd} = \mu_0 \mu^2$ (μ_0 is the vacuum permeability). We take all the dipoles to be aligned along a dipole-alignment axis $\hat{\mathcal{E}}$ by means of a large external field taken to lie in the x, z plane (illustrated in Fig. 1). We thus envision experiments conducted in a fixed frame of reference, with the polarization orientation free to be tuned relative to this axis.
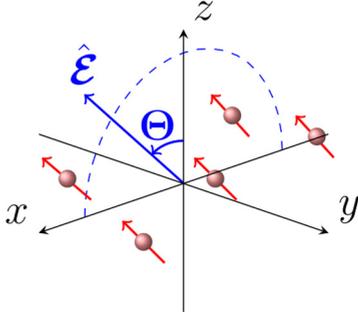
FIG. 1. A visualization of dipoles (red) aligned with an external field along the dipole-alignment axis $\hat{\mathcal{E}}$ (blue) in the laboratory coordinate frame.

Close to local thermal equilibrium, reequilibration processes are encapsulated by transport coefficients (e.g., viscosity, thermal conductivity, etc.) derivable from a microscopic picture by methods established by Chapman and Enskog [12]. The development we present here closely follows that of [26].

Within length scales on the order of the atomic mean free path, atomic interactions are dominated by collisional processes. The local distribution of atoms in flow thus has dynamics well described by the Boltzmann transport equation [27,28]

$$\left(\frac{\partial}{\partial t} + v_i \partial_i\right) f(\boldsymbol{r}, \boldsymbol{v}) = \mathcal{C}[f(\boldsymbol{r}, \boldsymbol{v})], \tag{1a}$$

$$\mathcal{C}[f] = \int d\Omega' \frac{d\sigma}{d\Omega'}$$
$$\times \int d^3 v_1 |\boldsymbol{v} - \boldsymbol{v}_1|(f' f_1' - f f_1), \tag{1b}$$

where $f(\boldsymbol{r}, \boldsymbol{v})$ is the phase-space distribution function and $\mathcal{C}[f]$ is the two-body collision integral. We adopt the convention that all repeated indices are summed over unless otherwise specified, and primes denote postcollision velocities for pairs of atoms colliding with incoming velocities $\boldsymbol{v}$ and $\boldsymbol{v}_1$. We also adopt the compact notation $f_1 = f(\boldsymbol{r}, \boldsymbol{v}_1)$ and $f' = f(\boldsymbol{r}, \boldsymbol{v}')$. The gas number density is given by

$$n(\boldsymbol{r}, t) = \frac{\rho(\boldsymbol{r}, t)}{m} = \int d^3 v f(\boldsymbol{r}, \boldsymbol{v}, t), \tag{2}$$

which at thermal equilibrium is dependent on only temperature $n_0 = n_0(\beta)$. Thermal equilibrium also imposes a Boltzmann velocity distribution,

$$f_0(\boldsymbol{u}, \beta) = n_0(\beta) c_0(\boldsymbol{u}, \beta) = n_0(\beta) \left(\frac{m\beta}{2\pi}\right)^{3/2} \exp\left(-\frac{m\beta}{2}\boldsymbol{u}^2\right), \tag{3}$$

where $\beta = (k_B T)^{-1}$, $\boldsymbol{u}^2 = u_k u_k$, and $\boldsymbol{u}(\boldsymbol{r}) = \boldsymbol{v} - \boldsymbol{U}(\boldsymbol{r})$ is the peculiar velocity, defined as the molecular velocity $\boldsymbol{v}$ relative to the flow velocity,

$$\boldsymbol{U}(\boldsymbol{r}, t) = \frac{1}{n(\boldsymbol{r}, t)} \int d^3 v f(\boldsymbol{r}, \boldsymbol{v}, t) \boldsymbol{v}. \tag{4}$$

In close-to-equilibrium scenarios, we can consider the out-of-equilibrium atomic distribution to take the form

$$f(\boldsymbol{r}, \boldsymbol{u}, \beta) \approx f_0(\boldsymbol{u}, \beta)[1 + \Phi(\boldsymbol{r}, \boldsymbol{u}, \beta)], \tag{5}$$

with a perturbation function Φ that must satisfy

$$\int d^3 u f_0(\boldsymbol{u}) \Phi(\boldsymbol{r}, \boldsymbol{u}, \beta) m = 0, \tag{6a}$$

$$\int d^3 u f_0(\boldsymbol{u}) \Phi(\boldsymbol{r}, \boldsymbol{u}, \beta) m \boldsymbol{u} = 0, \tag{6b}$$

$$\int d^3 u f_0(\boldsymbol{u}) \Phi(\boldsymbol{r}, \boldsymbol{u}, \beta) \frac{1}{2} m \boldsymbol{u}^2 = 0 \tag{6c}$$

as a result of mass, momentum, and energy conservation, respectively. Enskog's prescription of successive approximations then renders the Boltzmann equation, to leading nontrivial order, as

$$\left(\frac{\partial}{\partial t} + v_i \partial_i\right) f_0 \approx C[f_0 \Phi]. \tag{7}$$

Physically, this approximation is motivated by establishing a separation of scales between phenomena of interest. We are concerned with the regime in which macroscopic fluid dynamics is governed by length scales λ (e.g., wavelengths) much larger than the mean free path L of its constituent atoms (i.e., the regime of small Knudsen number $\mathrm{Kn} = L\lambda^{-1} \ll 1$). Furthermore, the period over which such dynamics occurs is much longer than the timescales associated with collisions. Therefore, Eq. (7) effectively makes an adiabatic approximation that separates the macro- and microscale phenomena. We refer to the fluid dynamics as occurring on "macroscales," whereas collisional interactions are said to occur on "microscales."

Under the approximation described above, the left-hand side of Eq. (7) equates to

$$\left(\frac{\partial}{\partial t} + v_k \partial_k\right) f_0 = f_0 \big[V_k \partial_k(\ln T) + m\beta W_{k\ell} D_{k\ell}\big], \tag{8}$$

where

$$V_i(\boldsymbol{u}) \equiv \left(\frac{m\beta \boldsymbol{u}^2}{2} - \frac{5}{2}\right) u_i, \tag{9a}$$

$$W_{ij}(\boldsymbol{u}) \equiv u_i u_j - \frac{1}{3}\delta_{ij}\boldsymbol{u}^2, \tag{9b}$$

$$D_{ij}(\boldsymbol{U}) \equiv \frac{1}{2}(\partial_j U_i + \partial_i U_j) - \frac{1}{3}\delta_{ij}\partial_k U_k. \tag{9c}$$

The derivation of this result is detailed in Appendix A. The collision integral on the right-hand side of Eq. (7) is then

$$C[f] \approx \int d^3 u_1 |\boldsymbol{u} - \boldsymbol{u}_1| f_0(\boldsymbol{u}) f_0(\boldsymbol{u}_1) \int d\Omega' \frac{d\sigma}{d\Omega'} \Delta\Phi, \tag{10}$$

where $\Delta\Phi = \Phi' + \Phi_1' - \Phi - \Phi_1$. Since Eq. (10) is linear in Φ and Eq. (8) is linear in the quantities $\partial_i \ln T$ and $\partial_j U_i$, one can infer an *ansatz* for the scalar function Φ of the form

$$\Phi(\boldsymbol{u}, \beta) = \mathcal{B}_k \partial_k(\ln T) + m\beta \mathcal{A}_{k\ell} D_{k\ell}, \tag{11}$$

where $\boldsymbol{\mathcal{B}}$ (vector) and $\boldsymbol{\mathcal{A}}$ (two-rank tensor) are functions of $\boldsymbol{u}$ and β. The *ansatz* above allows a separation of Eq. (7) into an equation in velocity gradients and that in temperature gradients,

$$f_0 W_{k\ell} D_{k\ell} \approx C[f_0 \mathcal{A}_{k\ell}] D_{k\ell}, \tag{12a}$$

$$f_0 V_k \partial_k(\ln T) \approx C[f_0 \mathcal{B}_k] \partial_k(\ln T). \tag{12b}$$

which upon a comparison of the terms, further motivate us to write $\mathcal{B}$ and $\mathcal{A}$ as

$$\mathcal{A}_{ij}(\boldsymbol{u}, n_0, \beta) = W_{k\ell}(\boldsymbol{u})a_{k\ell ij}(u, n_0, \beta), \qquad (13a)$$

$$\mathcal{B}_i(\boldsymbol{u}, n_0, \beta) = V_j(\boldsymbol{u})b_{ji}(u, n_0, \beta), \qquad (13b)$$

where $u = |\boldsymbol{u}|$ and the coefficients $a_{k\ell mn}(u, n_0, \beta)$ and $b_{k\ell}(u, n_0, \beta)$ are introduced as variational *ansatze*. These variational coefficients can, in general, be expressed as an infinite linear combination of Sonine polynomials (also known as associated Laguerre polynomials). The assumption of a low-temperature gas, however, allows us to approximate $\boldsymbol{a}$ and $\boldsymbol{b}$ with only the first term in the summation series, which is u independent. Such an approximation has been shown to have good accuracy (relative errors of $\sim 1\%$) in computing transport coefficients for gases of isotropic scatterers [28–30]. We are thus left with

$$\Phi(\boldsymbol{u}, \beta) = V_\ell(\boldsymbol{u})b_{\ell k}(n_0, \beta)\partial_k(\ln T)$$
$$+ m\beta W_{ij}(\boldsymbol{u})a_{ijk\ell}(n_0, \beta)D_{k\ell}. \qquad (14)$$

The coefficients a and b are determined for a particular gas by the microscopic scattering theory of the constituents, a task to which we now turn.

III. THERMAL CONDUCTIVITY IN DIPOLAR GASES

Thermal conduction in a dilute gas arises through a transfer of kinetic energy by kinetic transport of the gaseous atoms, out of a region of fluid, resulting in a heat flux [19],

$$J_i(\boldsymbol{r}, t) = \int d^3u \, f(\boldsymbol{r}, \boldsymbol{u}, t)\frac{1}{2}m\boldsymbol{u}^2 u_i. \qquad (15)$$

For a first-order approximation, we adopt the *ansatz* in Eq. (11) to compute the integral above. The $\mathcal{A}$ associated term does not contribute to the heat-flux integral, leaving us with

$$J_i = \frac{m}{2} \int d^3u f_0(\boldsymbol{u})[1 + \Phi(\boldsymbol{u})]\boldsymbol{u}^2 u_i$$
$$= \left(\frac{k_B m \beta}{2} \int d^3u \, f_0(\boldsymbol{u})\boldsymbol{u}^2 u_i V_k b_{kj}\right)\partial_j T, \qquad (16)$$

where the local temperature $T(\boldsymbol{r}, t)$ is written in terms of its kinetic definition,

$$\frac{3}{2}k_B T = \frac{1}{n(\boldsymbol{r}, t)} \int d^3u \, f(\boldsymbol{r}, \boldsymbol{u}, t)\frac{1}{2}m\boldsymbol{u}^2. \qquad (17)$$

Additionally, we say that this flow of kinetic energy occurs across a temperature gradient via Fourier's law of heat conduction,

$$J_i = -\kappa_{ij}\partial_j T, \qquad (18)$$

where $\boldsymbol{\kappa}$ is the thermal conductivity, a two-rank tensor. A comparison of Eqs. (16) and (18) then tells us that the thermal conductivity is found via the integral

$$\kappa_{ij} = -\left(\frac{k_B m \beta}{2} \int d^3u \, f_0(\boldsymbol{u})\boldsymbol{u}^2 u_i V_k\right)b_{kj} = -\frac{5n_0 k_B}{2m\beta}b_{ij}, \qquad (19)$$

assuming knowledge of the coefficients b_{kj}.

The transport of kinetic energy across a temperature gradient is brought about by the flow of atoms mediated by collisions, allowing use of the Boltzmann equation to derive $\boldsymbol{b}(u)$, with the first-order Chapman-Enskog expansion. Referring back to Eq. (12b), one finds that it is formally mathematically inconsistent but holds in an average sense over the atomic distribution after multiplying Eq. (12b) by $V_i(\boldsymbol{u})$ and integrating over $\boldsymbol{u}$. This gives

$$\left(\int d^3u \, f_0(\boldsymbol{u})V_i(\boldsymbol{u})V_j(\boldsymbol{u})\right)\partial_j(\ln T)$$
$$\approx \left(\int d^3u \, V_i(\boldsymbol{u})C[f_0 V_k]\right)b_{kj}\partial_j(\ln T), \qquad (20)$$

where the coefficients of $\partial_j(\ln T)$ satisfy the relation

$$N_{ik}b_{kj} = \delta_{ij}, \qquad (21a)$$

$$N_{ik} \equiv \frac{2m\beta}{5n_0} \int d^3u \, V_i C[f_0 V_k]. \qquad (21b)$$

The integral terms above are made complicated by the highly anisotropic differential cross section for dipolar bosons, for which the appropriately symmetrized scattering amplitude is provided in closed form as [11]

$$f_B(\hat{\boldsymbol{u}}'_r, \hat{\boldsymbol{u}}_r) = \frac{a_d}{\sqrt{2}}\left(\frac{4}{3} - 2a_s - \frac{2(\hat{\boldsymbol{u}}_r \cdot \hat{\mathcal{E}})^2 + 2(\hat{\boldsymbol{u}}'_r \cdot \hat{\mathcal{E}})^2 - 4(\hat{\boldsymbol{u}}_r \cdot \hat{\mathcal{E}})(\hat{\boldsymbol{u}}'_r \cdot \hat{\mathcal{E}})(\hat{\boldsymbol{u}}_r \cdot \hat{\boldsymbol{u}}'_r)}{1 - (\hat{\boldsymbol{u}}_r \cdot \hat{\boldsymbol{u}}'_r)^2}\right), \qquad (22)$$

where $\boldsymbol{u}_r = \boldsymbol{u} - \boldsymbol{u}_1$. This provides us the differential cross section via $d\sigma/d\Omega' = |f_B(\hat{\boldsymbol{u}}'_r, \hat{\boldsymbol{u}}_r)|^2$, with which the N_{ik} terms are evaluated as

$$\mathcal{N}_{11} = -\frac{256}{15} + \frac{256a_d[3\cos(2\Theta) - 1]}{225a}$$
$$- \frac{512a_d^2[3\cos(2\Theta) + 13]}{4725a^2}, \qquad (23a)$$

$$\mathcal{N}_{13} = -\frac{256a_d \sin(2\Theta)}{75a} + \frac{512a_d^2 \sin(2\Theta)}{1575a^2}, \qquad (23b)$$

$$\mathcal{N}_{22} = -\frac{256}{15} + \frac{512a_d}{225a} - \frac{8192a_d^2}{4725a^2}, \qquad (23c)$$

with the additional relations

$$\mathcal{N}_{33}(\Theta) = \mathcal{N}_{11}(\Theta - \pi/2), \qquad (24a)$$

$$\mathcal{N}_{12}(\Theta) = \mathcal{N}_{23}(\Theta) = 0, \qquad (24b)$$

$$\mathcal{N}_{ij}(\Theta) = \mathcal{N}_{ji}(\Theta), \qquad (24c)$$

where we have cast N_{ik} in terms of the adimensional functions

$$\mathcal{N}_{ij} = \frac{1}{a^2 n_0}\sqrt{\frac{m\beta}{\pi}}N_{ij}. \qquad (25)$$

The details of the evaluation of these integrals are provided in Appendix B, following the successful methods developed
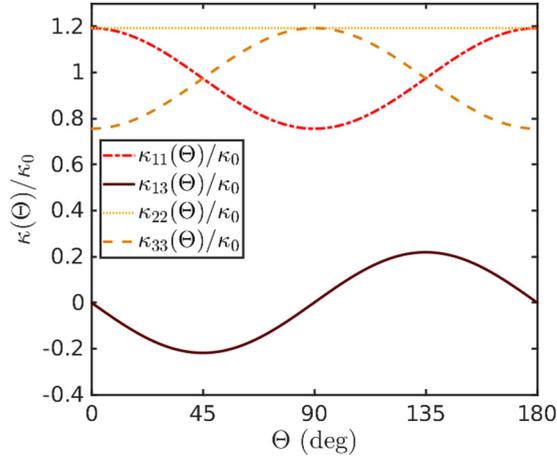
FIG. 2. The unit-free thermal-conductivity tensor elements $\boldsymbol{\kappa}/\kappa_0$ as a function of the dipole-alignment angle Θ, as defined in Eq. (26) for native ^{164}Dy ($a = 92a_0$). The tensor elements κ_{11}/κ_0 (solid dark red line), κ_{13}/κ_0 (dot-dashed red line), and κ_{22}/κ_0 (dashed orange line) display a sinusoidal Θ dependence, whereas κ_{33}/κ_0 (dotted yellow line) is Θ independent due to the coordinate frame definition. The parameters considered here are for ^{164}Dy with $a_d/a \approx 199/92$, taken from Ref. [6].

in [4]. It then follows that the thermal-conductivity tensor is given as

$$
\boldsymbol{\kappa}(\Theta) = -\frac{5k_B}{2a^2\sqrt{\pi m \beta}} \mathcal{N}^{-1}(\Theta)
$$

$$
= -\frac{5k_B}{2a^2\sqrt{\pi m \beta}}
\begin{pmatrix}
\frac{\mathcal{N}_{33}}{\mathcal{N}_{11}\mathcal{N}_{33}-\mathcal{N}_{13}^2} & 0 & \frac{\mathcal{N}_{13}}{\mathcal{N}_{13}^2-\mathcal{N}_{11}\mathcal{N}_{33}} \\
0 & \frac{1}{\mathcal{N}_{22}} & 0 \\
\frac{\mathcal{N}_{13}}{\mathcal{N}_{13}^2-\mathcal{N}_{11}\mathcal{N}_{33}} & 0 & \frac{\mathcal{N}_{11}}{\mathcal{N}_{11}\mathcal{N}_{33}-\mathcal{N}_{13}^2}
\end{pmatrix}.
$$

(26)

The structure of the tensor above and Eq. (18) imply that a temperature gradient along x could result in a thermal flux along z and vice versa. In the event that the dipoles are aligned along $\hat{z}$, that is, $\Theta = 0$, the Cartesian axes are the principal axes of $\boldsymbol{\kappa}$. This situation leaves us with only two unique, nontrivial thermal conductivities, $\kappa_{xx} = \kappa_{yy} \neq \kappa_{zz}$.

We plot in Fig. 2 the coefficients in Eq. (26) with values normalized by the isotropic coefficient κ/κ_0 [31], where

$$
\kappa_0 = \frac{75k_B}{256r_{\text{eff}}^2\sqrt{\pi m \beta}},
$$

(27)

where $r_{\text{eff}}^2 = 2a^2 + 8a_d^2/45$ is an effective isotropic radius obtained from an angular average of the dipolar differential cross section. The coefficients are plotted with the scattering and dipole lengths of native ^{164}Dy ($a = 92a_0$ and $a_d = 199a_0$, where a_0 is the Bohr radius) [6], which showcases the functional dependence on the angle Θ between the polarization and the laboratory z axis.

IV. EQUATIONS OF MOTION

Having derived the transport tensor of thermal conductivity, macroscopic gas dynamics can now be studied under the lens of a continuum fluid formulation. The dynamics of

fluids is characterized by spatial and temporal variations of macroscopic quantities such as the fluid mass density ρ (2), flow-velocity $\boldsymbol{U}$ (4), and temperature

$$
T(\boldsymbol{r}, t) = \frac{2}{3n(\boldsymbol{r}, t)k_B} \int d^3v f(\boldsymbol{r}, \boldsymbol{v}, t) \frac{1}{2}m\boldsymbol{u}^2.
$$

(28)

The associated hydrodynamic phenomena are well modeled, even in ultracold systems [32], by the continuum conservation equations [19]

$$
\frac{\partial \rho}{\partial t} + \partial_j(\rho U_j) = 0,
$$

(29a)

$$
\frac{\partial}{\partial t}(\rho U_i) + \partial_j(\rho U_j U_i) = \partial_j \sigma_{ij},
$$

(29b)

$$
\frac{\partial}{\partial t}(\rho T) + \partial_j(\rho T U_j) = \frac{2m}{3k_B}(\sigma_{ij}\partial_j U_i - \partial_j J_j),
$$

(29c)

where ∂_i denotes a derivative with respect to the coordinate r_i ($i = 1, 2, 3$) and m is the atomic mass. These equations are, in order, referred to as the continuity, Navier-Stokes, and energy-balance equations. As we saw in the previous section, atom-atom collisions in the gas result in thermal transport and viscous effects, included into Eqs. (29) via the heat-flux vector J_j and pressure tensor [33]

$$
\sigma_{ij} = -P\delta_{ij} + \tau_{ij},
$$

(30a)

$$
\tau_{ij} = \mu_{ijk\ell}\partial_\ell U_k,
$$

(30b)

where P is the thermodynamic pressure, τ_{ij} is the viscous stress tensor, and $\mu_{ijk\ell}$ is the viscosity tensor. For the time being, we focus on the influence of thermal conductivity by assuming that all second derivatives of the flow velocity are small, effectively rendering the viscous stress terms negligible (i.e., $\tau_{ij} \approx 0$). Consideration of the anisotropic viscosity is left to future work.

V. DIFFUSION OF A HOT SPOT

As an example of anisotropy due to the thermal-conductivity tensor, we consider a simple uniform-gas experiment in which a localized temperature hot spot is induced, for example, by heating the gas locally with a focused laser and then allowed to diffuse. For simplicity, we assume that the temperature field is excited perturbatively so that the temperature dynamics is described by its deviation from the uniform background temperature T_0, $T(\boldsymbol{r}, t) = T_0[1 + \epsilon(\boldsymbol{r}, t)]$. This permits a linearization of Eq. (29c) to first order in ϵ, which gives

$$
\frac{\partial \epsilon}{\partial t} \approx -\frac{2}{3}\partial_j U_j + \frac{2}{3n_0 k_B}\kappa_{ij}\partial_i\partial_j\epsilon.
$$

(31)

At the onset of the hot spot, the flow velocity $\boldsymbol{U}$ is taken to be negligible, thus rendering the heat equation as

$$
\frac{\partial \epsilon}{\partial t} = \mathcal{D}_{ij}\partial_i\partial_j\epsilon
$$

(32)

in terms of a thermal-diffusivity tensor

$$
\mathcal{D}_{ij} \equiv \frac{2}{3n_0 k_B}\kappa_{ij}.
$$

(33)
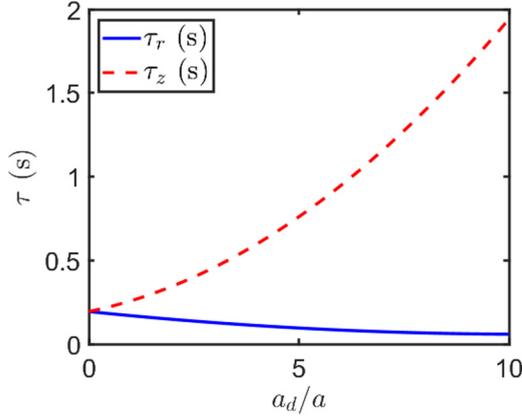
FIG. 3. Thermal relaxation timescales τ_r and τ_z vs the reduced dipole length a_d/a. The axial timescale τ_z is seen to be drastically larger than the radial timescale τ_r for large values of the reduced dipole length.

We model the initial hot spot as described by a Gaussian of width σ,

$$\epsilon(\boldsymbol{r}, t = 0) = \epsilon_0 e^{-\frac{r^2}{2\sigma^2}}. \qquad (34)$$

Utilizing a Fourier expansion, we obtain the time-dependent solution to Eq. (32),

$$\epsilon(\boldsymbol{r}, t) = \epsilon_0 \int \frac{\sigma^3 d^3 K}{(2\pi)^{3/2}} e^{-\frac{1}{2}K^2\sigma^2} e^{-(\boldsymbol{K}^T \boldsymbol{\mathcal{D}} \boldsymbol{K})t} e^{i\boldsymbol{K}\cdot\boldsymbol{r}}. \qquad (35)$$

The integral above can be evaluated analytically to get

$$\epsilon(\boldsymbol{r}, t) = \frac{\epsilon_0 \sigma^3}{\sqrt{8 \det(\boldsymbol{M})}} \exp\left(-\frac{\boldsymbol{r}^T \boldsymbol{M}^{-1} \boldsymbol{r}}{4}\right), \qquad (36a)$$

$$\boldsymbol{M} \equiv \frac{1}{2}\sigma^2 \mathbb{I} + \boldsymbol{\mathcal{D}}t, \qquad (36b)$$

where $\mathbb{I}$ is the identity matrix. The solution above is further simplified if we assume that the dipoles define the z axis, which is done here without loss of generality. The diffusion tensor is now diagonal with only two distinct elements, $\mathcal{D}_{11} = \mathcal{D}_{22}$ and $\mathcal{D}_{33}$. Thus, diffusions in the radial (perpendicular to the dipole alignment) and axial (parallel to the dipole alignment) directions occur with the respective different characteristic timescales

$$\tau_r \equiv \frac{\sigma^2}{2\mathcal{D}_{11}} = \frac{128(315a^2 - 42aa_d + 32a_d^2)}{7875 r_{\text{eff}}^2} \tau_0, \qquad (37a)$$

$$\tau_z \equiv \frac{\sigma^2}{2\mathcal{D}_{33}} = \frac{128(315a^2 + 84aa_d + 20a_d^2)}{7875 r_{\text{eff}}^2} \tau_0, \qquad (37b)$$

with $\tau_0 = \sigma^2 r_{\text{eff}}^2 n_0 \sqrt{\pi m \beta}$, which dictate the Gaussian hot-spot relaxation time along the radial and axial directions, respectively. These timescales are, of course, identical in the limit of vanishing dipole moment $a_d = 0$. Their difference is quite pronounced, however, as a_d increases, as illustrated in Fig. 3. Figure 3 uses the experimental parameters in Table I and a hot spot of initial width $\sigma = 5L \approx 0.6$ (mm). It is apparent that the diffusion occurs far more rapidly in the axial direction when dipolar scattering is significant.

TABLE I. Experimental parameter values. Da $= 1.661 \times 10^{-27}$ kg stands for daltons (atomic mass unit), $a_0 = 5.292 \times 10^{-11}$ m is the Bohr radius, and $\mu_B = 9.274 \times 10^{-24}$ J/T is the Bohr magneton.

Parameter	Symbol	Value	Unit
Atomic mass number	A	164	Da
Magnetic moment	μ	10	μ_B
Dipole length	a_d	199	a_0
Equilibrium number density	n_0	10^{13}	cm^{-3}
Equilibrium gas temperature	T_0	300	nK

With the dipoles aligned along $\hat{z}$, the explicit time evolution of the hot spot is given by

$$\epsilon(\boldsymbol{r}, t) = \frac{\epsilon_0 \exp\left(-\frac{x^2 + y^2}{2\sigma^2\left(1 + \frac{t}{\tau_r}\right)} - \frac{z^2}{2\sigma^2\left(1 + \frac{t}{\tau_z}\right)}\right)}{\sqrt{\left(1 + \frac{t}{\tau_z}\right)^2 \left(1 + \frac{t}{\tau_r}\right)}}. \qquad (38)$$

Figure 4 visualizes the anisotropy of thermal relaxation by showing the temperature field variation ϵ in the x, z plane. We plot the time evolution of ϵ in Fig. 4, up to the geometric mean of the two timescales in three panels ($t = 0$, $\sqrt{\tau_r \tau_z}/2$, $\sqrt{\tau_r \tau_z}$), where we have set $a = 0$ to accentuate the dipolar anisotropy. With the parameters in Table I, the timescales take values $\tau_r = 0.0667$ s and $\tau_z = 0.667$ s. The Gaussian hot spot clearly elongates along the x direction over time, demonstrating an observable effect of anisotropic thermal conductivity during thermal diffusion in the fluid. This could be observed in ultracold-atom experiments with time-of-flight imaging, which extracts the gas momentum distribution. Exciting such a temperature hot spot would create additional peaks in the momentum distribution that our theory predicts would thermalize anisotropically.

VI. DISCUSSION AND CONCLUSION

Normal-phase gases of ultracold dipolar atoms present a vast arena for anisotropic dynamical phenomena. In large enough samples, a continuum description of these systems is warranted, permitting fluid dynamics studies. The fluid equations of motion are, however, complete only upon specification of the transport tensors, which govern the finite-time dispersive processes in the fluid. In this work, we have used the Chapman-Enskog procedure to derive analytic expressions for the anisotropic transport tensor of thermal conductivity, induced by collisions between dipolar bosons. By construction, each tensor element is a function of the dipole-alignment angle and functionally dependent on the ratio of dipole length to scattering length.

We then analyzed the anisotropic effects of these thermal conductivities in the thermal relaxation of a Gaussian hot spot, where time-dependent solutions were derived from a linearization of the viscosity-free fluid equations. We found that an initially isotropic hot spot would disperse preferentially in a direction orthogonal to the dipole orientation, opening the possibility for controlling heat transport with the dipole-alignment direction.
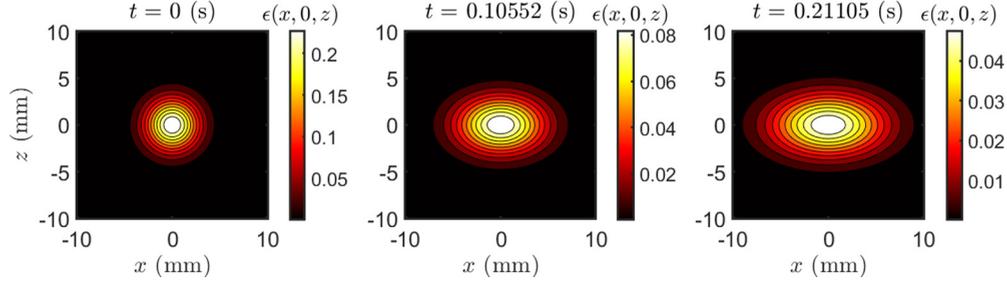
FIG. 4. Stroboscopic evolution of the temperature-field variation $\epsilon(\mathbf{r}, t)$ at times $t = 0, 0.106, 0.211$ s (from left to right), visualized along a 2D slice in the x, z plane. The initial peak temperature fluctuation amplitude is set to $\epsilon_0 = 0.25$, and the color scale for each plot is rescaled for visual clarity at each time instance.

A comprehensive fluid description will, of course, require the transport tensor of viscosity to also be derived. The analytic techniques presented here permit this derivation, which will be a subject of future work. Another possible extension of this work is to include quantum statistical effects in computing the transport coefficients, as done in Refs. [32,34], but with the dipolar cross section of Ref. [11]. These effects might become relevant at temperatures closer to quantum degeneracy. Finally, we note that recent experiments have realized long-lived three-dimensional polar molecular samples by microwave shielding [35,36] or dc electric fields [37], promising larger and tunable electric dipole moments in collisional dipolar gases. These systems would serve as ideal platforms for experimental investigations of dipolar fluid dynamics.

APPENDIX A: THE FIRST-ORDER CHAPMAN-ENSKOG APPROXIMATION TO THE BOLTZMANN EQUATION

This Appendix details the derivation of the left-hand side of the Boltzmann equation under the Chapman-Enskog expansion to first order [26]. We can first write this expression as

$$\left(\frac{\partial}{\partial t} + v_i \partial_i\right) f_0 = f_0 \left(\frac{\partial}{\partial t} + v_i \partial_i\right) \ln f_0$$

$$= f_0 \left(\frac{D}{Dt} + u_i \partial_i\right) \ln f_0, \qquad (A1)$$

where we defined the material derivative

$$\frac{D}{Dt} \equiv \frac{\partial}{\partial t} + U_j \partial_j. \qquad (A2)$$

From Eq. (3), it follows that

$$\ln f_0 = \frac{3}{2} \ln \frac{m}{2\pi} + \ln(n_0 \beta^{3/2}) - \frac{m\beta}{2} \mathbf{u}^2, \qquad (A3)$$

so

$$\left(\frac{\partial}{\partial t} + v_i \partial_i\right) f_0 = f_0 \left(\frac{D}{Dt} + u_i \partial_i\right) \left[\ln(n_0 \beta^{3/2}) - \frac{m\beta}{2} \mathbf{u}^2\right]. \qquad (A4)$$

At local thermal equilibrium as prescribed by f_0, the equations of conservation [Eq. (29)] reduce to

$$\frac{D}{Dt} n_0 = -n_0 \partial_j U_j, \qquad (A5a)$$

$$\frac{D}{Dt} U_i = -\frac{1}{n_0} \partial_i \left(\frac{n_0}{m\beta}\right), \qquad (A5b)$$

$$\frac{D}{Dt} \beta = \frac{2}{3} \beta \partial_j U_j, \qquad (A5c)$$

from which the equations of continuity and energy balance can be combined to give the relation

$$\frac{D}{Dt} \ln(n_0 \beta^{3/2}) = 0, \qquad (A6)$$

identifying the quantity $\ln(n_0 \beta^{3/2})$ as an adiabatic invariant. This simplifies the expression to

$$\left(\frac{D}{Dt} + u_i \partial_i\right) f_0 = f_0 u_j \partial_j \ln(n_0 \beta^{3/2}) - f_0 \left(\frac{D}{Dt} + u_i \partial_i\right) \frac{m\beta}{2} \mathbf{u}^2. \qquad (A7)$$

Applying the material derivative to the term in $\mathbf{u}^2$ gives

$$\frac{D}{Dt}\left(\frac{m\beta}{2} \mathbf{u}^2\right) = \frac{m}{2}\left(\mathbf{u}^2 \frac{D\beta}{Dt} + \beta \frac{D\mathbf{u}^2}{Dt}\right)$$

$$= m\beta\left(\frac{1}{3} \mathbf{u}^2 \partial_i U_i - u_i \frac{DU_i}{Dt}\right)$$

$$= m\beta\left[\frac{1}{3} \mathbf{u}^2 \partial_i U_i + \frac{u_i}{n_0} \partial_i \left(\frac{n_0}{m\beta}\right)\right]$$

$$= \frac{1}{3} m\beta \mathbf{u}^2 \partial_i U_i + u_i \partial_i \ln(n_0 T); \qquad (A8)$$

thus, the left-hand side of the Boltzmann equation becomes

$$\left(\frac{D}{Dt} + v_i \partial_i\right) \ln f_0$$

$$= u_i \partial_i \left(\frac{5}{2} \ln \beta - \frac{m\beta}{2} \mathbf{u}^2\right) - \frac{1}{3} m\beta \mathbf{u}^2 \partial_i U_i$$

$$= \frac{1}{\beta}\left(\frac{5}{2} - \frac{m\beta}{2} \mathbf{u}^2\right) u_i \partial_i \beta + m\beta\left(u_i u_j \partial_j U_i - \frac{1}{3} \mathbf{u}^2 \partial_i U_i\right)$$

$$= \left(\frac{m\beta}{2} \mathbf{u}^2 - \frac{5}{2}\right) u_i \partial_i (\ln T) + m\beta\left(u_i u_j - \frac{1}{3} \delta_{ij} \mathbf{u}^2\right)$$

$$\times \left(\frac{\partial_j U_i + \partial_i U_j}{2} - \frac{1}{3} \delta_{ij} \partial_k U_k\right), \qquad (A9)$$
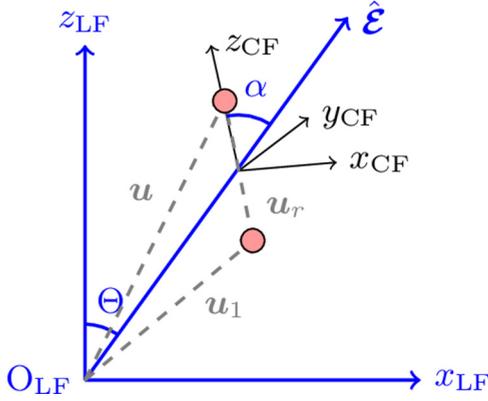
FIG. 5. The collision frame (black) defined in the laboratory frame (blue) via the relative velocities between two colliding partners (red spheres). The angle α is defined as that between vectors $\boldsymbol{u}_r$ and $\hat{\boldsymbol{\mathcal{E}}}$.

which is the form presented in Eq. (8) of the main text.

APPENDIX B: EVALUATION OF THE COLLISION INTEGRAL FOR THERMAL CONDUCTION

The collision integral to be computed is written as

$$N_{ik} = \frac{2m\beta}{5n_0} \int d^3u V_i(\boldsymbol{u}) C[f_0 V_k] \qquad \text{(B1)}$$

$$= \frac{2m\beta}{5n_0} \int d^3u \, V_i(\boldsymbol{u}) \int d^3u_1 |\boldsymbol{u} - \boldsymbol{u}_1| f_0(\boldsymbol{u}) f_0(\boldsymbol{u}_1)$$

$$\times \int d\Omega' \frac{d\sigma}{d\Omega'} \Delta V_k. \qquad \text{(B2)}$$

In considering both the thermal motion of the atoms and collisional processes, it is convenient to first define the velocities in terms of center-of-mass (c.m.) and relative (r) coordinates,

$$\boldsymbol{u}_{\text{c.m.}} = \frac{\boldsymbol{u} + \boldsymbol{u}_1}{2}, \qquad \text{(B3a)}$$

$$\boldsymbol{u}_{\text{r}} = \boldsymbol{u} - \boldsymbol{u}_1, \qquad \text{(B3b)}$$

which allows the product of equilibrium distributions to be recast as

$$f_0(\boldsymbol{u}) f_0(\boldsymbol{u}_1) = f_{\text{c.m.}}(\boldsymbol{u}_{\text{c.m.}}) f_{\text{r}}(\boldsymbol{u}_{\text{r}}), \qquad \text{(B4a)}$$

$$f_{\text{c.m.}}(\boldsymbol{u}_{\text{c.m.}}) \equiv n_0 \left(\frac{m\beta}{\pi}\right)^{3/2} \exp\left(-m\beta u_{\text{c.m.}}^2\right), \quad \text{(B4b)}$$

$$f_{\text{r}}(\boldsymbol{u}_{\text{r}}) = n_0 \left(\frac{m\beta}{4\pi}\right)^{3/2} \exp\left(-\frac{m\beta}{4} u_{\text{r}}^2\right). \quad \text{(B4c)}$$

Furthermore, the anisotropy of the dipolar differential cross section has us consider two distinct coordinate frames: (1) the

laboratory frame (LF) defined by the dipole-alignment axis $\hat{\boldsymbol{\mathcal{E}}}$ lying along the $x_{\text{LF}}, z_{\text{LF}}$ plane (Fig. 1) and (2) the collision frame (CF) defined by aligning the $\hat{z}_{\text{CF}}$ axis in the direction of relative incoming velocities $\boldsymbol{u}_r$ for two colliding atoms (visualization in Fig. 5). We perform the collision integral in coordinates defined with respect to the laboratory frame.

To transform between coordinate frames, we construct a frame-rotation matrix of direction cosines,

$$R_{\text{CF}\rightarrow\text{LF}} = \begin{pmatrix} \hat{x}_{\text{LF}} \cdot \hat{x}_{\text{CF}} & \hat{x}_{\text{LF}} \cdot \hat{y}_{\text{CF}} & \hat{x}_{\text{LF}} \cdot \hat{z}_{\text{CF}} \\ \hat{y}_{\text{LF}} \cdot \hat{x}_{\text{CF}} & \hat{y}_{\text{LF}} \cdot \hat{y}_{\text{CF}} & \hat{y}_{\text{LF}} \cdot \hat{z}_{\text{CF}} \\ \hat{z}_{\text{LF}} \cdot \hat{x}_{\text{CF}} & \hat{z}_{\text{LF}} \cdot \hat{y}_{\text{CF}} & \hat{z}_{\text{LF}} \cdot \hat{z}_{\text{CF}} \end{pmatrix}, \qquad \text{(B5)}$$

that takes the vector $\hat{\boldsymbol{u}}_r'$ from the CF to the LF. The differential scattering cross section is then also required to be expressed in LF coordinates during integration of the collision integral. To do so, we utilize the coordinate-independent form of the scattering amplitude for bosons f_B (22) and express that in terms of our desired coordinates, which allows us to compute the differential cross section $d\sigma/d\Omega'$. The above coordinate transformations are sufficient for us to now compute the collision integrals.

Expanding in terms of the c.m. and r coordinates of Eq. (B3), the collision integral becomes

$$N_{ik} = \frac{2m\beta}{5n_0} \int d^3u_{\text{c.m.}} f_{\text{c.m.}}(\boldsymbol{u}_{\text{c.m.}})$$

$$\times \int d^3u_{\text{r}} f_{\text{r}}(\boldsymbol{u}_{\text{r}}) u_{\text{r}} V_i(\boldsymbol{u}_{\text{c.m.}}, \boldsymbol{u}_{\text{r}}) \int d\Omega' \frac{d\sigma}{d\Omega'} \Delta V_k. \quad \text{(B6)}$$

Collisions result in the variation

$$\Delta V_k = \Delta \left[\left(\frac{m\beta \boldsymbol{u}^2}{2} - \frac{5}{2} \right) u_k \right] = \frac{m\beta}{2} \Delta(\boldsymbol{u}^2 u_k), \qquad \text{(B7)}$$

where the velocity terms are written in terms of CF and LF coordinates as

$$u_i = u_{\text{c.m.},i} + \tfrac{1}{2} u_{\text{r},i}, \qquad \text{(B8a)}$$

$$u_{1,i} = u_{\text{c.m.},i} - \tfrac{1}{2} u_{\text{r},i}, \qquad \text{(B8b)}$$

$$\boldsymbol{u}^2 = \boldsymbol{u}_{\text{c.m.}}^2 + \tfrac{1}{4}\boldsymbol{u}_{\text{r}}^2 + u_{\text{c.m.},j} u_{\text{r},j}, \qquad \text{(B8c)}$$

$$\boldsymbol{u}_1^2 = \boldsymbol{u}_{\text{c.m.}}^2 + \tfrac{1}{4}\boldsymbol{u}_{\text{r}}^2 - u_{\text{c.m.},j} u_{\text{r},j}, \qquad \text{(B8d)}$$

which gives the expansion

$$\Delta(\boldsymbol{u}^2 u_i) = \boldsymbol{u}'^2 u_i' + \boldsymbol{u}_1'^2 u_{1,i}' - \boldsymbol{u}^2 u_i - \boldsymbol{u}_1^2 u_{1,i}$$

$$= \boldsymbol{u}_{\text{c.m.}} \cdot \left(\boldsymbol{u}_r' u_{r,i}' - \boldsymbol{u}_{\text{r}} u_{\text{r},i} \right). \qquad \text{(B9)}$$

The integral over postcollision velocities is then performed as

$$\int d\Omega' \frac{d\sigma}{d\Omega'} \Delta V_k \equiv \frac{m\beta}{2} \int d\Omega' \frac{d\sigma}{d\Omega'} \Delta(\boldsymbol{u}^2 u_k), \qquad \text{(B10)}$$

which, when plugged back into Eq. (B6) and evaluated, gives the result in Eq. (23) and expressions thereafter.

[1] L. Chomaz, I. Ferrier-Barbut, F. Ferlaino, B. Laburthe-Tolra, B. L. Lev, and T. Pfau, arXiv:2201.02672.

[2] A. G. Sykes and J. L. Bohn, Phys. Rev. A **91**, 013625 (2015).

[3] Y. Tang, A. G. Sykes, N. Q. Burdick, J. M. DiSciacca, D. S. Petrov, and B. L. Lev, Phys. Rev. Lett. **117**, 155301 (2016).

[4] R. R. W. Wang, A. G. Sykes, and J. L. Bohn, Phys. Rev. A **102**, 033336 (2020).

[5] R. R. W. Wang and J. L. Bohn, Phys. Rev. A **103**, 063320 (2021).

[6] Y. Tang, A. Sykes, N. Q. Burdick, J. L. Bohn, and B. L. Lev, Phys. Rev. A **92**, 022703 (2015).

[7] T. Maier, I. Ferrier-Barbut, H. Kadau, M. Schmitt, M. Wenzel, C. Wink, T. Pfau, K. Jachymski, and P. S. Julienne, Phys. Rev. A **92**, 060702(R) (2015).

[8] E. Lucioni, L. Tanzi, A. Fregosi, J. Catani, S. Gozzini, M. Inguscio, A. Fioretti, C. Gabbanini, and G. Modugno, Phys. Rev. A **97**, 060701(R) (2018).

[9] G. Durastante, C. Politi, M. Sohmen, P. Ilzhöfer, M. J. Mark, M. A. Norcia, and F. Ferlaino, Phys. Rev. A **102**, 033330 (2020).

[10] A. Patscheider, L. Chomaz, G. Natale, D. Petter, M. J. Mark, S. Baier, B. Yang, R. R. W. Wang, J. L. Bohn, and F. Ferlaino, Phys. Rev. A **105**, 063307 (2022).

[11] J. L. Bohn and D. S. Jin, Phys. Rev. A **89**, 022702 (2014).

[12] S. Chapman and T. G. Cowling, *The Mathematical Theory of Non-uniform Gases: An Account of the Kinetic Theory of Viscosity, Thermal Conduction and Diffusion in Gases* (Cambridge University Press, Cambridge, 1990).

[13] H. Hanley, R. McCarty, and E. Cohen, Physica (Amsterdam) **60**, 322 (1972).

[14] N. F. Mott and H. S. W. Massey, *The Theory of Atomic Collisions*, 2nd ed. (Oxford University Press, Oxford, 1949).

[15] M. K. Dehkordi, M. A. Shahzamanian, M. R. Abolhasani, and M. Elahi, J. Phys.: Conf. Ser. **400**, 012029 (2012).

[16] S. I. Braginskii and M. A. Leontovich, *Reviews of Plasma Physics* (Consultants Bureau, New York, 1965).

[17] U. Daybelge, J. Appl. Phys. **41**, 2130 (1970).

[18] D. Bruno, C. Catalfamo, A. Laricchiuta, D. Giordano, and M. Capitelli, Phys. Plasmas **13**, 072307 (2006).

[19] S. De Groot and P. Mazur, *Non-equilibrium Thermodynamics*, Dover Books on Physics (Dover Publications Inc., New York, 2013).

[20] C. Salueña, A. Perez-Madrid, and J. Rubi, J. Chem. Phys. **96**, 6950 (1992).

[21] Y. J. Suh and K. Cho, Mater. Trans. **56**, 1262 (2015).

[22] R. B. Bird, W. E. Stewart, and E. N. Lightfoot, *Transport Phenomena Revised*, 2nd ed. (Wiley, Hoboken, NJ, 2006).

[23] B. Bottin, D. V. Abeele, T. E. Magin, and P. Rini, Prog. Aerospace Sci. **42**, 38 (2006).

[24] J. L. Plawsky, *Transport Phenomena Fundamentals* (CRC Press, Boca Raton, FL, 2009).

[25] G. A. Truskey, F. Yuan, and D. F. Katz, *Transport Phenomena in Biological Systems* (Pearson, 2010).

[26] J. W. Bond, Jr., K. M. Watson, and J. A. Welch, Jr., *Atomic Theory of Gas Dynamics*, Addison-Wesley Series in Aerospace Science (Addison-Wesley Publishing Company, Inc., Reading, MA, 1965).

[27] K. Huang, *Statistical Mechanics* (Wiley, New York, 1963), p. 10.

[28] F. Reif, *Fundamentals of Statistical and Thermal Physics* (Waveland, Long Grove, IL, 2009).

[29] C. L. Pekeris and Z. Alterman, Proc. Natl. Acad. Sci. U.S.A. **43**, 998 (1957).

[30] S. Loyalka, E. Tipton, and R. Tompson, Phys. A (Amsterdam, Neth.) **379**, 417 (2007).

[31] The coefficient κ_0 is exactly the result of Chapman and Enskog [12] but modified to include the quantum-mechanical scattering length instead of a classical hard-sphere radius.

[32] T. Nikuni and A. Griffin, J. Low Temp. Phys. **111**, 793 (1998).

[33] C. S. Jog, *Fluid Mechanics*, Volume 2, *Foundations and Applications of Mechanics* (Cambridge University Press, Cambridge, 2015).

[34] E. A. Uehling, Phys. Rev. **46**, 917 (1934).

[35] L. Anderegg, S. Burchesky, Y. Bao, S. S. Yu, T. Karman, E. Chae, K.-K. Ni, W. Ketterle, and J. M. Doyle, Science **373**, 779 (2021).

[36] A. Schindewolf, R. Bause, X.-Y. Chen, M. Duda, T. Karman, I. Bloch, and X.-Y. Luo, Nature **607**, 677 (2022).

[37] J.-R. Li, W. G. Tobias, K. Matsuda, C. Miller, G. Valtolina, L. D. Marco, R. R. W. Wang, L. Lassablière, G. Quéméner, J. L. Bohn, and J. Ye, Nat. Phys. **17**, 1144 (2021).